Volcanic history of the Imbrium basin: A close-up view from the lunar rover Yutu

Jinhai Zhang[a], Wei Yang[a], Sen Hu[a], Yangting Lin[a,1], Guangyou Fang[b], Chunlai Li[c], Wenxi Peng[d], Sanyuan Zhu[e], Zhiping He[f], Bin Zhou[b], Hongyu Lin[g], Jianfeng Yang[h], Enhai Liu[i], Yuchen Xu[a], Jianyu Wang[f], Zhenxing Yao[a], Yongliao Zou[c], Jun Yan[c], and Ziyuan Ouyang[j]

[a]Key Laboratory of Earth and Planetary Physics, Institute of Geology and Geophysics, Chinese Academy of Sciences, Beijing 100029, China; [b]Institute of Electronics, Chinese Academy of Sciences, Beijing 100190, China; [c]National Astronomical Observatories, Chinese Academy of Sciences, Beijing 100012, China; [d]Institute of High Energy Physics, Chinese Academy of Sciences, Beijing 100049, China; [e]Key Laboratory of Mineralogy and Metallogeny, Guangzhou Institute of Geochemistry, Chinese Academy of Sciences, Guangzhou 510640, China; [f]Key Laboratory of Space Active Opto-Electronics Technology, Shanghai Institute of Technical Physics, Chinese Academy of Sciences, Shanghai 200083, China; [g]The Fifth Laboratory, Beijing Institute of Space Mechanics & Electricity, Beijing 100076, China; [h]Xi'an Institute of Optics and Precision Mechanics, Chinese Academy of Sciences, Xi'an 710119, China; [i]Institute of Optics and Electronics, Chinese Academy of Sciences, Chengdu 610209, China; and [j]Institute of Geochemistry, Chinese Academy of Science, Guiyang 550002, China

Edited by Mark H. Thiemens, University of California, San Diego, La Jolla, CA, and approved March 24, 2015 (received for review February 13, 2015)

We report the surface exploration by the lunar rover Yutu that landed on the young lava flow in the northeastern part of the Mare Imbrium, which is the largest basin on the nearside of the Moon and is filled with several basalt units estimated to date from 3.5 to 2.0 Ga. The onboard lunar penetrating radar conducted a 114-m-long profile, which measured a thickness of ∼5 m of the lunar regolith layer and detected three underlying basalt units at depths of 195, 215, and 345 m. The radar measurements suggest underestimation of the global lunar regolith thickness by other methods and reveal a vast volume of the last volcano eruption. The in situ spectral reflectance and elemental analysis of the lunar soil at the landing site suggest that the young basalt could be derived from an ilmenite-rich mantle reservoir and then assimilated by 10–20% of the last residual melt of the lunar magma ocean.

volcanic history | Imbrium basin | lunar rover Yutu | lunar penetrating radar | Chang'e-3 mission

The surface of the Moon is covered by regolith, a mixed layer of fine-grained lunar soil and ejecta deposits, which is crucial to understanding the global composition of the Moon. The lunar regolith has also recorded the complex history of the surface processes, and it is the main reservoir of ^{3}He and other solar wind gases. The thickness of the lunar regolith was estimated to be from 2 to 8 m in the maria and up to 8–16 m in the highland areas using various methods (1), including crater morphology (2, 3), seismology with low spatial resolution (4), radar wave scattering (5), and microwave brightness temperature (6). However, no in situ measurement of spectral reflectance, elemental compositions, lunar regolith thickness, or subsurface structures has been carried out.

The surface of the Moon is dominated with numerous large basins. They were formed about 3.9 Ga (7, 8), probably by the late heavy bombardment, and then filled with dark lava flows derived from partial melting of the lunar mantle, within a period mainly during 3.8–3.1 Ga (7). The Imbrium basin is the largest and was formed on Procellarum KREEP [potassium (K), rare earth elements (REE), and phosphorus (P)] Terrane (9), a unique terrain highly enriched in U, Th, and K radionuclides and other incompatible trace elements referred to as KREEP (10) and considered as the last residual melt of the Lunar Magma Ocean (11). The presence of the KREEPy materials, indicated by high concentrations of radionuclides U, Th, and K (9), around the rims of the Imbrium basin suggests that they are likely the basin-forming ejecta deposits. At least three main lava flows, dated from 3.5 Ga to 2.0–2.3 Ga (7, 12), have been recognized in Mare Imbrium with distinct FeO and TiO_2 concentrations (13, 14), which brought up interior information of this KREEP-rich terrain. The old and low-Ti basalt unit has been sampled by the Apollo 15 mission that landed at the eastern rim of the Imbrium basin. Information of other lava flows in Mare Imbrium was obtained only by remote sensing from orbit. On December 14, 2013, Chang'e-3 successfully landed on the young and high-Ti lava flow in the northeastern Mare Imbrium, about 10 km south from the old low-Ti basalt unit (Fig. 1).

The lunar rover Yutu (named for the jade rabbit on the Moon in a Chinese fairy tale) was equipped with an active particle-induced X-ray spectrometer (APXS), a visible to near-infrared (450–945 nm) imaging spectrometer and short-wave infrared (900–2,395 nm) spectrometer (VNIS), and a lunar penetrating radar (LPR), accompanied by a stereo camera and a navigating camera. Originally, the mission planned to have the lunar rover measure chemical and mineral compositions of the lunar soil and various types of ejecta rocks and to carry out a LPR profile of the lunar regolith and subsurface structures in the first 3 mo. The mission was scheduled to extend up to 1 y and to explore the old low-Ti lava flow ∼10 km north. Unfortunately, some of Yutu's mechanical parts failed to move just before the rover prepared for sleeping at the end of the second month due to unknown faults probably in the control system. During the first 2 mo, Yutu successfully carried out two APXS and four VNIS analyses of the lunar soil and performed a 114-m-long LPR profile along the rover track in the landing area (Fig. 2). These in situ measurements

Significance

After the Apollo and Luna missions, which were flown about 40 years ago, the Moon was explored only from orbit. In addition, no samples were returned from the young and high-FeO and TiO_2 mare basalt in the northern Imbrium basin. Such samples are important to understand the formation and evolution of the Procellarum KREEP [potassium (K), rare earth elements (REE), and phosphorus (P)] terrain, a key terrain highly enriched in radioactive nuclides. The Chang'e-3 mission carried out the first in situ analyses of chemical and mineral compositions of the lunar soil and ground-based measurements of the lunar regolith and the underlying basalt units at this specific site. The lunar regolith layer recorded the surface processes of the Moon, whereas the basalt units recorded the volcanic eruption history.

Author contributions: Y.L., C.L., Y.Z., J. Yan, and Z.O. designed research; J.Z., W.Y., S.H., Y.L., and W.P. performed research; G.F., W.P., Z.H., H.L., J. Yang, E.L., and J.W. contributed new reagents/analytic tools; J.Z., W.Y., S.H., Y.L., S.Z., B.Z., Y.X., and Z.Y. analyzed data; and J.Z., W.Y., S.H., Y.L., and Y.X. wrote the paper.

The authors declare no conflict of interest.

This article is a PNAS Direct Submission.

Freely available online through the PNAS open access option.

[1]To whom correspondence should be addressed. Email: linyt@mail.igcas.ac.cn.

This article contains supporting information online at www.pnas.org/lookup/suppl/doi:10.1073/pnas.1503082112/-/DCSupplemental.

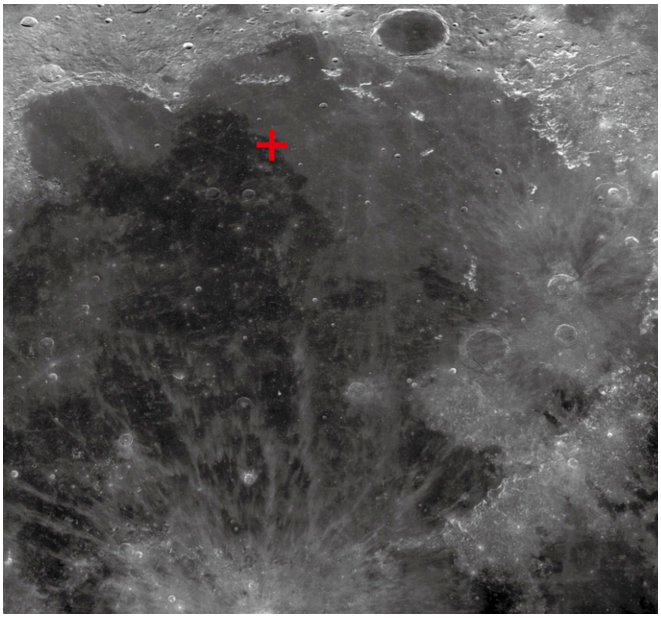

Fig. 1. The landing site of Chang'e-3 (red cross), on the high-Ti basalt (dark gray) near the boundary in contact with the low-Ti basalt (light gray). The background image was taken by Chang'e-1.

provide insights into the volcanic history of Mare Imbrium and the ground-truth data for calibration of the orbital data.

Chemical Compositions

The chemical compositions of the lunar soil have been measured with the onboard APXS equipped on the robotic arm (Table 1), and detailed data processing is given in *SI Appendix*. The X-ray spectra of the lunar soil were emitted from the surface within a diameter of 6 cm, displaying clear peaks of Mg, Al, Si, Ca, Ti, K, Cr, Fe, Sr, and Zr and detection of Y and Nb (*SI Appendix*, Fig. S3). The quantitative compositions of the lunar soil were calibrated with 10 working references covering the compositional ranges of the lunar soil, after correction for background, peak overlapping, and decay of the ^{55}Fe and ^{109}Cd sources. The two analyses, carried out in different locations, are nearly identical to each other within the analytical uncertainties, confirming the analytical reproducibility. The lunar soil contains higher TiO_2 (4.0–4.3 wt %) and FeO (21.3–22.1 wt %) but lower Al_2O_3 (10.5–11.5 wt %) compared with the Apollo and Luna soil samples (*SI Appendix*, Fig. S6). The composition of the lunar soil could represent that of the basalt beneath, suggested by its high FeO and TiO_2 contents. This is confirmed by the compositional mapping of the rims and proximal ejecta of small impacts (0.4–4 km in diameter) on the same high-Ti basalt unit, which show the upper limits of 20 wt % FeO and 4–7 wt % TiO_2 (14). The intermediate concentration of TiO_2, compared with the gap between 4 and 7 wt % TiO_2 for Apollo and Luna mare basalts (15) (Fig. 3), probably indicates a distinct type of mare basalt. Based on the correlation between K and Th (16), 4 ppm Th of the lunar soil was estimated, which is slightly higher than the remote sensing value (~2 ppm Th) in Mare Imbrium (17). The incompatible lithophile trace elements Zr, Y, and Nb are enriched by factors of 0.10–0.12, 0.11–0.18, and 0.17 relative to the referred composition of KREEP (10), respectively. In addition, the concentration of K is 0.18–0.22 × KREEP. Such a nearly flat KREEP-normalized pattern of the lunar soil suggests that these incompatible lithophile trace elements can be attributed to assimilation of 10–20% of KREEP component. A scenario is that the basalt was derived via partial melting of ilmenite-rich mantle reservoir and then contaminated by the residual KREEP layer beneath the ferroan anorthosite crust as it ascended to the surface. Alternatively, the basalt was formed via partial melting of a mantle reservoir that had mixed with sinking dense ilmenite-rich KREEPy rock.

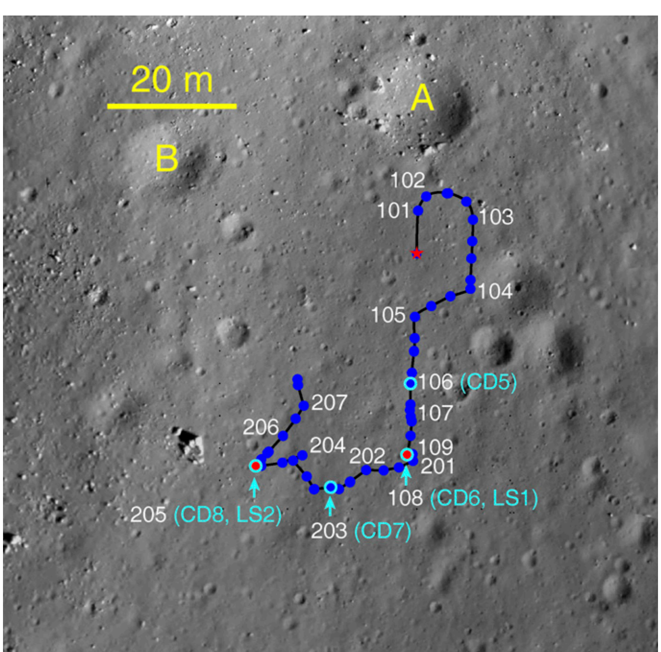

Fig. 2. Chang'e-3 landing site and the rover Yutu's track. Crater A is blocky, indicating penetration through the regolith. Crater B is the largest one without blocks in the landing area. The APXS (LS1–LS2) and VNIS (CD5–CD8) analysis positions and the rover navigation points are marked. The image was composed from the series images taken by the Chang'e-3 landing camera.

Mineral Abundances and Optical Maturity Index

Four reflection spectra of the lunar soil have been acquired with the onboard VNIS, and the data processing is given in *SI Appendix*. The calibrated spectra are similar to the laboratory measurements of Apollo mare soil samples, showing absorption at 1 μm and 2 μm responding to the presence of pyroxene and plagioclase (*SI Appendix*, Fig. S11). The decoded average mineral composition of the soil is 17.9 vol % pyroxene (13.0–20.6 vol %) and 16.4 vol % plagioclase (15.0–17.5 vol %). This mineral composition

Table 1. Chemical compositions of the lunar soil measured with APXS

Sample name	LS1	±	LS2	±
SiO_2	42.8		43.2	
MgO	9.9	1.5	8.9	1.9
Al_2O_3	11.5	0.9	10.5	1.0
K_2O	0.18	0.01	0.15	0.01
CaO	10.4	0.3	10.9	0.4
TiO_2	4.0	0.2	4.3	0.2
FeO	21.3	1.7	22.1	1.9
Total	100.0		100.0	
Cr, ppm	877	162	825	161
Sr, ppm	139	19	198	29
Y, ppm	34	10	54	13
Zr, ppm	200	26	168	49
Nb, ppm	13	2	14	10

In wt %, normalized to 100 wt %. LS1, lunar soil 1; LS2, lunar soil 2.

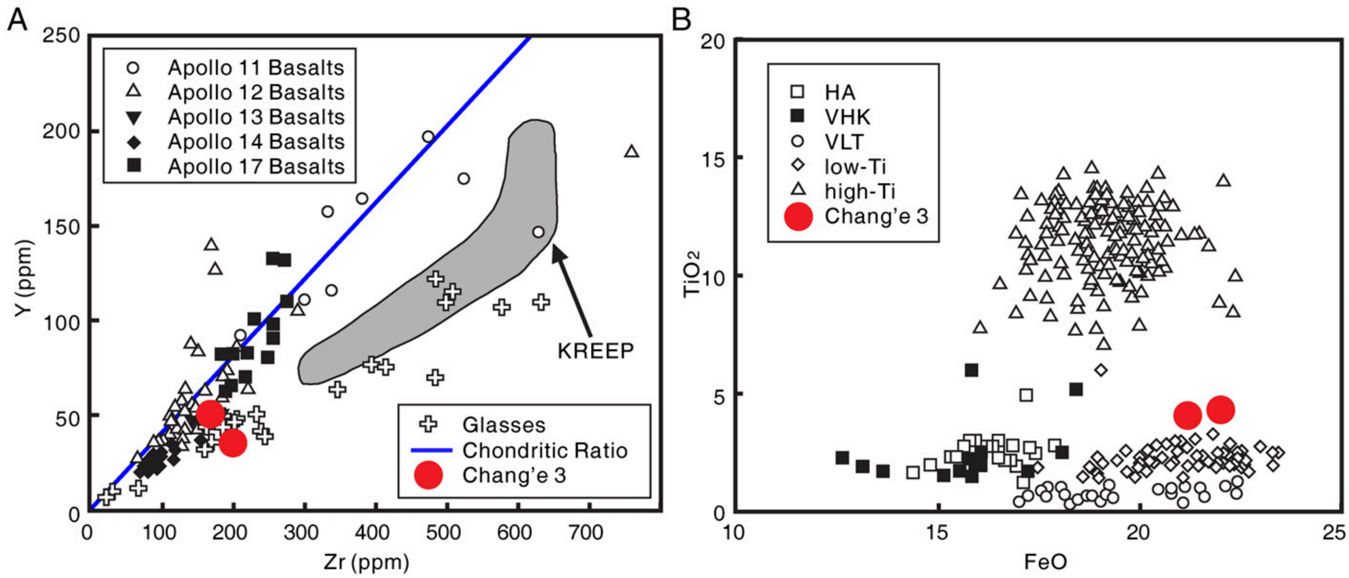

Fig. 3. Compositions of the lunar soil at the landing site. (*A*) Y and Zr plot close to the mixing line with KREEP, different from Apollo basalts (14). (*B*) The FeO and TiO_2 contents plot in the gap between the high-Ti and low-Ti basalt samples (15).

is consistent with the average Apollo mare soils that consist of 16.3 vol % plagioclase and 18.6 vol % pyroxenes (1). The Apollo mare soils also contain abundant impact glass and volcanic glass with minor olivine (~3.4 vol %); however, they cannot be decoded from the reflectance spectra. Furthermore, the FeO and TiO_2 concentrations of the lunar soil can be

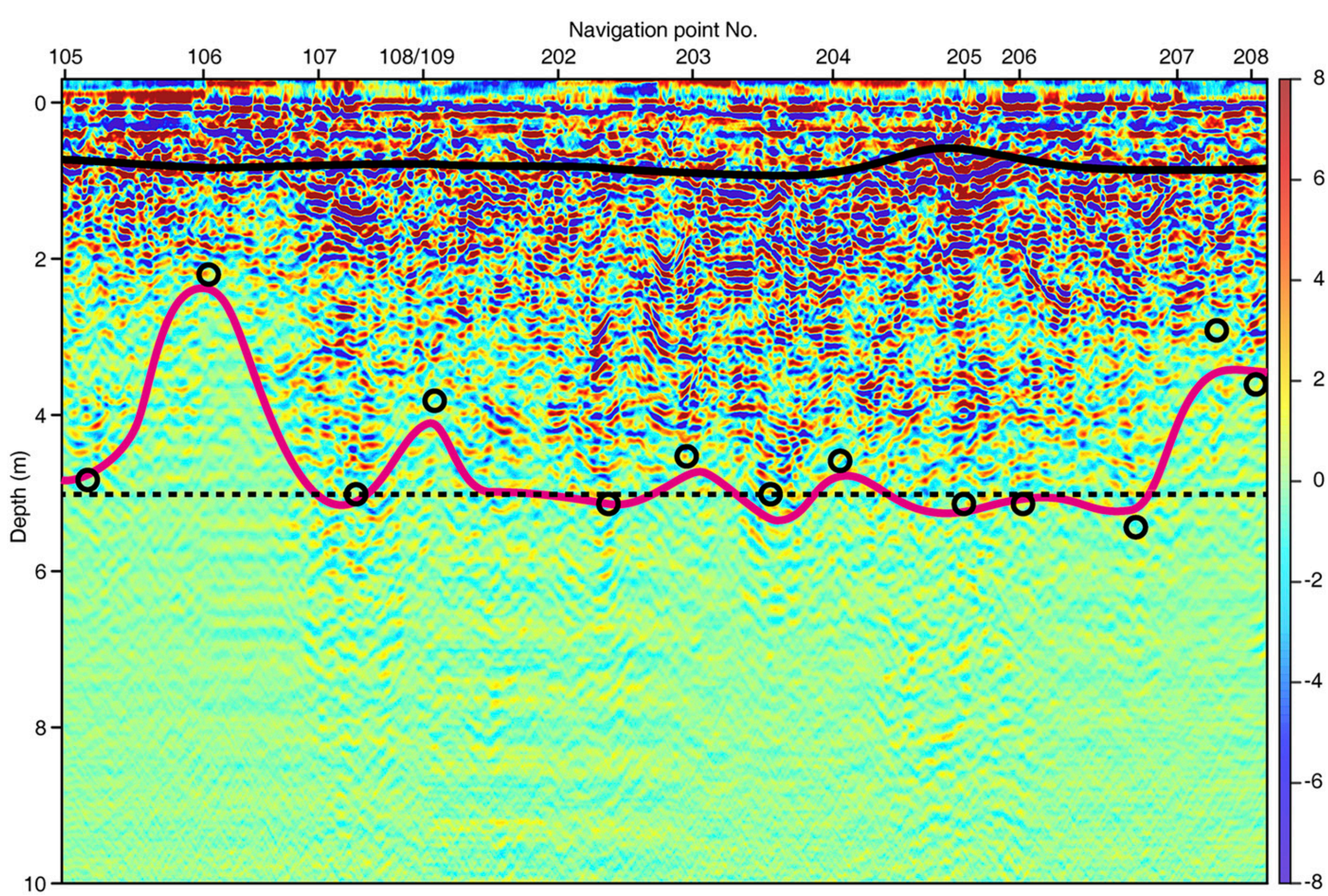

Fig. 4. Migration result of channel 2B of LPR. The profile is about 73 m long. Bold black and pink curves denote the lunar soil sublayer and regolith bottoms picked up manually, respectively. Bold black circles are the depths of lunar regolith picked up from the key traces by time–frequency analyses after migration (shown in *SI Appendix*, Fig. S19). The dashed black line (at 5 m) denotes the best depth estimation of the lunar regolith at the research area.

estimated from the corrections between the compositions and the reflectance spectrum parameters of the Apollo soils (*SI Appendix*, Fig. S9), which are 18.9 wt % (18.7–19.5 wt %) and 6.6 wt % (5.3–9.0 wt %), respectively. The estimated TiO_2 contents are somewhat higher than the APXS analyses, likely due to the shadow of the rough lunar soil surface (*SI Appendix*, Fig. S8). The estimated FeO contents are consistent with the APXS analyses within analytical uncertainties. The space weathering effect (darkening and reddening of the spectra) of the lunar soil can be indicated by the optical maturity index (18), which ranges from 0.098 to 0.158 with an exception of 0.312 for CD005 (*SI Appendix*, Table S2). The higher values of the optical maturity index and the spectral reflectance of CD005 may be due to blowing the top dusts off the lunar surface by the rocket during the descent of Chang'e-3 because CD005 is located closest to the lander (*SI Appendix*, Table S2). The optical maturity index values of CD006–CD008 suggest submature or mature lunar soil, undistinguishable from the Apollo mare soils. This is inconsistent with the rocky surface and the presence of abundant rocks in the lunar soil at the landing site (*SI Appendix*, Fig. S2), which is suggestive of a young age for the Chang'e-3 landing site. However, it has been noticed that there was no clear correlation between the optical maturity index and the ages of the Apollo mare soils (18).

Lunar Regolith Layer Thickness

The lunar regolith layer and the underlying basalt units at the landing site have been detected by the onboard LPR, which has two frequency channels, i.e., channel 1 at 60 MHz and channel 2 at 500 MHz. The echoes were processed using preprocessing, migration and time–frequency analysis methods that are commonly used in seismic exploration (*SI Appendix*). Fig. 4 displays the LPR profile of channel 2 with a total distance of 73 m along the Yutu's track. The relative dielectric constant ε_r increases from 2.1 at the surface to 6.5 at a depth of 10 m, based on the function of lunar soil density with depth (19) and a model of the lunar regolith. We propose that the homogeneous uppermost sublayer contains 5.7 vol % of basaltic blocks determined from the high-resolution images of the landing camera (*SI Appendix*, Fig. S2). Then, we assume that the rock debris content of the lunar regolith increases with depth to 100% at 10 m deep. The high-frequency LPR echoes clearly exhibit an uneven bottom of the lunar regolith, and the depth varies from 2.2 m to 5.4 m with a median value of ∼5 m (Fig. 4).

The thickness of the lunar regolith layer can also be constrained by high-resolution morphology of craters taken by the landing camera of Yutu. There are two large craters in the landing region (Fig. 2). The larger one (crater A, 18 m in diameter) is blocky, indicative of penetrating the regolith layer and excavating the underlying bedrock, whereas the other (crater B, 13.7 m in diameter) has few blocks, and hence, it is inside the regolith layer. The depths of both craters were calculated to 3.7 m and 4.9 m using the impacting model of the lunar regolith (www.lpi.usra.edu/lunar/tools/lunarcratercalc/). The depths of 3.7 m and 4.9 m can be referred to as the range of the regolith layer thickness, which is consistent with the LPR measurement. The ground-based LPR measurement of the lunar regolith layer thickness clarifies the wide range in previous estimations from 2.6 m (20) to 7.5 m (21) using the crater morphology method, or 6.2 ± 2.0 m (5) and 6.4 ± 1.7 m (22) based on lunar radar sounder data, in the same young, high-Ti region of Mare Imbrium. A thickness of 8.5–12.2 m of the regolith layer in the Apollo highlands was measured with seismology (4), but the lunar regolith layer thickness of 2–8 m at the Apollo mare sites was estimated (1). In addition, a much thicker regolith (8–32 m, with a median depth of 11 m) was estimated in three Eratosthenian mare areas (2.0–2.5 Ga) (23). Based on the positive correlation between regolith layer thickness and age of the surface (5), the regolith layer thickness at the young Chang'e-3 landing site could be considered to be the minimum of the global surface because of its young age of 3.0 Ga (7) or 2.0–2.3 Ga (12). The thick regolith layer at the Chang'e-3 landing site may be partially attributed to the ejecta deposits from a crater ∼450 m in diameter, which locates ∼60 m west to the lander. However, the high-resolution descending images reveal no recognizable modification of the distribution pattern of small craters on the surface (Fig. 2). The thickness of ejecta deposits must be less than 20 cm; otherwise, the craters <0.5 m in diameter would have been buried. Hence, the echoes detected by the LPR are mainly from the regolith layer rather than the ejecta deposits of the nearby crater. The mean thicknesses of the lunar regolith layer at Apollo mare sites were generally reported to 2–8 m (1), and the lower range could be somewhat underestimated because these sites are significantly older (3.8–3.1 Ga). This is also confirmed by the blocky nature of the Chang'e landing site, which suggests a thinner regolith layer than the Apollo sites.

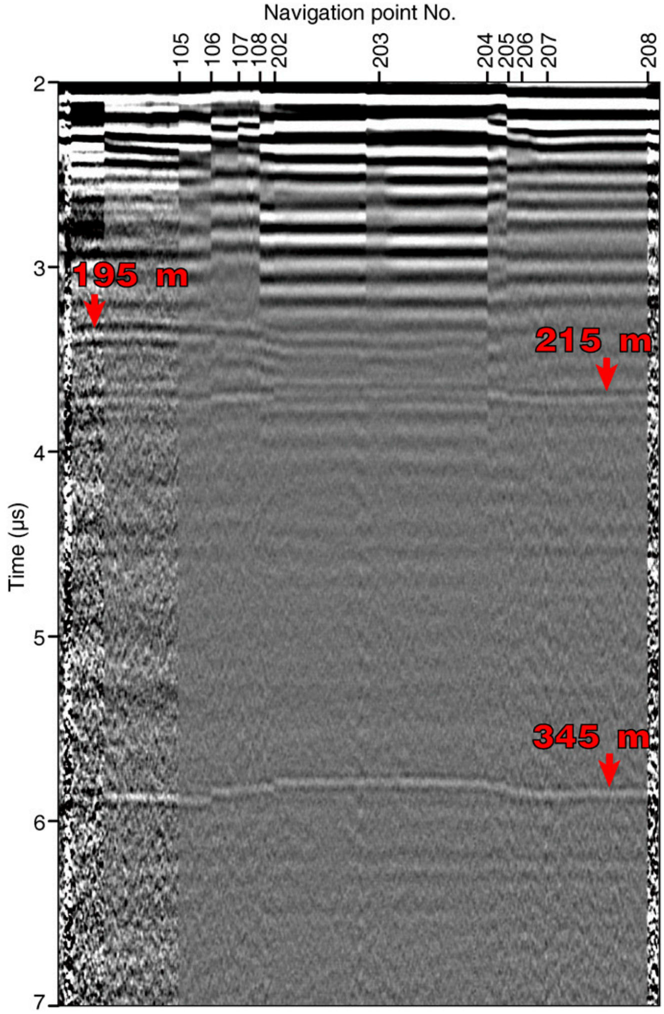

Fig. 5. The LPR profile of channel 1.

In Fig. 4, the uppermost sublayer (∼0.7 m in thickness) can be observed. The presence of this sublayer is independent of the model of the lunar regolith we used (*SI Appendix*, Figs. S16 and S17). This homogeneous sublayer likely represents the well–plowed-up top zone of the lunar regolith caused by small impacts. The measured thickness of ∼0.7 m of the sublayer is consistent with that of the homogeneous zone (∼60 cm) at the top of Apollo 17 deep drill cores (1).

Underlying Basalt Units

The underlying basalt units were probed by the low-frequency LPR echoes. Three obvious reflectors can be observed at depths of 195 m, 215 m, and 345 m (Fig. 5), using $\varepsilon_r = 6.5$ (1). These reflectors likely indicate buried regolith layers formed during flooding hiatus of lava flows in the northeastern Mare Imbrium. This is consistent with the presence of three main types of basalt units in Mare Imbrium, based on variation of FeO and TiO_2 contents (13, 14). These basalt units were dated 3.3–3.5 Ga, 3.0 Ga, and 2–2.5 Ga (7, 12, 24). The lava flows originated from the vent area near the crater Euler (over 700 km south to the landing site) and extended north 1,200 km, 600 km, and 400 km from older low-Ti basalts to the overlying high-Ti flows (*SI Appendix*, Fig. S1). The buried regolith layers between these basalt units are expected, produced by asteroid impacts during the time periods between the eruptions of the basalt units, which are likely responsible for these significant reflection horizons. Hence, the thickness of these three basalt units is 195 m, 20 m, and 130 m, from the top to the bottom, respectively.

Based on the effects of lava flow on lunar crater populations, the thickness of lava flows in the southwest Mare Imbrium were determined to 30–60 m (25) or six flow units with an average of 32–50 m (26). The much thicker uppermost basalt unit determined by Yutu's LPR suggests a sequence of lava flooding events (e.g., refs. 3–6) during a short period, and the individual flows cannot be detected by the LPR because of little regolith produced in the short hiatus. The total thickness of the top two basalt units (both high Ti) can be constrained by morphology of small craters with diameters of 0.4–4.0 km. The distribution of the TiO_2 contents of the rims and proximal ejecta deposits of these craters determined from compositional mapping data (14) revealed whether or not the craters have penetrated the overlying layer and excavated the bedrock beneath. The smallest craters with a diameter of 0.4–1.0 km show a peak at ∼5.0 wt % TiO_2 with a low-TiO_2 tail, whereas that of large craters has a low-TiO_2 peak at ∼2.5 wt % (*SI Appendix*, Fig. S7). The high-TiO_2 peak is similar to the in situ APXS analyses and the remote sensing results (27, 28). The low-TiO_2 tail of the smallest craters is due to excavating the underlying low-Ti basalt unit, as indicated by the low-TiO_2 peak for the larger craters (1–4 km in diameter) and the presence of old low-Ti basalt about 10 km north to the landing site. This result sets up a range of the total thickness of the upper two basalt units, from significantly larger than 109 m (depth of a crater with 0.4-km diameter) to obviously less than 270 m (depth of a crater with a 1-km diameter). This is consistent with the total thickness (210 m) of the upper two reflectors of LPR. Two subsurface layers in the eastern Mare Imbrium (36.0° N, 15.3° W) have been detected by lunar radar sounder on the Kaguya spacecraft, with depths of 250 m and 454–460 m (29). The footprint of the lunar radar sounder is located on the old low-Ti basalt unit (29), and the first reflector could be assigned to the third echo of Yutu's LPR. However, the depth of 250 m is nearly twice of the thickness of the old low-Ti basalt unit determined by Yutu's LPR. In addition, the deeper layer at 454–460 m measured by Kaguya spacecraft has not been detected by Yutu's LPR.

Conclusions

The chemical compositions of the lunar soil at the Chang'e-3 landing site were determined in situ by APXS, including trace elements of Zr, Sr, Y, and Nb. Its higher FeO (21.3–22.1 wt %) and TiO_2 contents (4.0–4.3 wt %) and lower Al_2O_3 content (10.5–11.5 wt %) compared with the Apollo and Luna soil samples suggest a new type of basalt beneath, which has not yet been sampled in previous missions. The nearly flat KREEP-normalized abundance pattern of K, Zr, Y, and Nb suggests assimilation of the underlying KREEP material. The mineral abundances decoded from the ground-based measurements of the reflectance spectra of the lunar soil are similar to Apollo mare soil.

The thickness of the lunar regolith layer was measured with the LPR to be ∼5 m. This is significantly larger than what we expected for a young mare site dated about 2.0–3.0 Ga (7, 12). Such a thick lunar regolith layer is unlikely attributed to ejecta deposits from a nearly crater because no significant modification on the surface was observed in the high-resolution images taken by the descending camera. In addition, an upper sublayer of ∼70 cm was detected, which has a feature of lacking rocks. This argues against a detectible layer of the ejecta deposit along the lunar rover's track. Our LPR imaging results show that the thickness of the global lunar regolith layer was underestimated in previous studies (e.g., refs. 1, 20).

The presence of three basalt units detected by the LPR is consistent with the distribution of three main basalt units in the northern Mare Imbrium (*SI Appendix*, Fig. S1). The thickness of 195 m of the top basalt unit indicates no significant cessation of volcanic eruption in the Imbrium basin until 2.0–3.0 Ga, different from a gradual cessation of magma eruption in the Imbrium basin (30). This could be at least partially attributed to high concentrations of radionuclides in the Procellarum KREEP Terrane. The high-Ti basalt was probably formed via partial melting of ilmenite-rich lunar mantle reservoir, followed by ascending to the Imbrium basin with 10–20% contamination of the KREEP material.

Methods

The chemical compositions of the lunar soils were determined from the APXS analyses, calibrated with two analyses of the onboard basaltic working reference and a set of standards that were measured in laboratory. All of the original APXS data are in 2B level and have been corrected for background and peak overlapping (for data processing details, see *SI Appendix*, S2).

The mineral abundances, optical maturity index, and the contents of FeO and TiO_2 of the lunar soil were achieved from the VNIS data in 2B level. The VNIS spectra were combined from those measured separately by the VIS/NIR imaging spectrometer (450–945 nm) and the shortwave IR (SWIR) (900–2395 nm), and they were reduced to repair bad lines and make flat field corrections and converted to reflectance. The Modified Gaussian Model was applied to decode the VNIS spectra, and the Apollo mare soils data were used to calibrate the results (for data handling, see *SI Appendix*, S4).

The lunar regolith layer was detected by the high-frequency channel (500 MHz, channel 2), and the depths of underlying basalt units were detected by the low-frequency channel (60 MHz, channel 1) of LPR on the Yutu rover. The 2B level data of channel 2 were processed using spherical spreading amplitude compensation and filtered by the second-order Butterworth filter. The time–frequency analysis was applied to the channel 2 data. The depths of the lunar soil sublayer and the lunar regolith bottom were estimated using the migration method. For channel 1, the 2B level data were filtered by band-pass Butterworth filter and 2D median filter (for full technical details, see *SI Appendix*, S5).

ACKNOWLEDGMENTS. We thank two anonymous reviewers for their constructive reviews. The Chang'e-3 mission was carried out by the Chinese Lunar Exploration Program, and the data were supplied by the Ground Research and Application System of the Chinese Lunar Exploration Program. This study was supported by the Key Research Program of the Chinese Academy of Sciences (KGZD-EW-603), National Natural Science Foundation of China (41273077, 41490631, 41221002, 41074092, and 41103031), and National Major Project of China (2011ZX05008-006). Numerical simulation of electromagnetic wavefields was performed in Computer Simulation Laboratory, Institute of Geology and Geophysics, Chinese Academy of Sciences.

1. Heiken G, Vaniman D, French BM (1991) *Lunar Sourcebook: A User's Guide to the Moon* (Cambridge University Press, Houston).
2. Quaide WL, Oberbeck VR (1968) Thickness determinations of the lunar surface layer from lunar impact craters. *J Geophys Res* 73(16):5247–5270.
3. Bart GD (2014) The quantitative relationship between small impact crater morphology and regolith depth. *Icarus* 235(E8):130–135.
4. Nakamura Y, Dorman J, Duennebier F, Lammlein D, Latham G (1975) Shallow lunar structure determined from the passive seismic experiment. *Moon* 13(1-3):57–66.

5. Shkuratov YG, Bondarenko NV (2001) Regolith layer thickness mapping of the Moon by radar and optical data. *Icarus* 149(2):329–338.
6. Fa W, Jin Y-Q (2010) A primary analysis of microwave brightness temperature of lunar surface from Chang-E 1 multi-channel radiometer observation and inversion of regolith layer thickness. *Icarus* 207(2):605–615.
7. Hiesinger H, Jaumann R, Neukum G, Head JW, III (2000) Ages of mare basalts on the lunar nearside. *J Geophys Res* 105(E12):29239–29275.
8. Geiss J, Rossi A (2013) On the chronology of lunar origin and evolution. *Astron Astrophys Rev* 21(1):1–54.
9. Jolliff BL, Gillis JJ, Haskin LA, Korotev RL, Wieczorek MA (2000) Major lunar crustal terranes: Surface expressions and crust-mantle origins. *J Geophys Res* 105(E2): 4197–4216.
10. Warren PH, Wasson JT (1979) The origin of KREEP. *Rev Geophys* 17(1):73–88.
11. Warren PH (1985) The magma ocean concept and lunar evolution. *Annu Rev Earth Planet Sci* 13(1):201–240.
12. Morota T, et al. (2011) Timing and characteristics of the latest mare eruption on the Moon. *Earth Planet Sci Lett* 302(3-4):255–266.
13. Bugiolacchi R, Guest JE (2008) Compositional and temporal investigation of exposed lunar basalts in the Mare Imbrium region. *Icarus* 197(1):1–18.
14. Kramer GY, Jolliff BL, Neal CR (2008) Searching for high alumina mare basalts using Clementine UVVIS and Lunar Prospector GRS data: Mare Fecunditatis and Mare Imbrium. *Icarus* 198(1):7–18.
15. Kramer GY, Jolliff BL, Neal CR (2006) Distinguishing high-alumina mare basalts using Clementine UVVIS and Lunar Prospector GRS data: Mare Moscoviense and Mare Nectaris. *J Geophys Res* 113(E1):E01002.
16. Gillis JJ, Jolliff BL, Korotev RL (2004) Lunar surface geochemistry: Global concentrations of Th, K, and FeO as derived from lunar prospector and Clementine data. *Geochim Cosmochim Acta* 68(18):3791–3805.
17. Yamashita N, et al. (2010) Uranium on the Moon: Global distribution and U/Th ratio. *Geophys Res Lett* 37(10):L10201.
18. Lucey PG, Blewett DT, Taylor GJ, Hawke BR (2000) Imaging of lunar surface maturity. *J Geophys Res* 105(E8):20377–20386.
19. Olhoeft GR, Strangway DW (1975) Dielectric properties of the first 100 meters of the Moon. *Earth Planet Sci Lett* 24(3):394–404.
20. Bart GD, Nickerson RD, Lawder MT, Melosh HJ (2011) Global survey of lunar regolith depths from LROC images. *Icarus* 215(2):485–490.
21. Oberbeck VR, Quaide WL (1968) Genetic implications of Lunar regolith thickness variations. *Icarus* 9(1-3):446–465.
22. Kobayashi T, Kim JH, Seung Ryeol L, Araki H, Ono T (2010) Simultaneous observation of Lunar Radar Sounder and Laser Altimeter of Kaguya for lunar regolith layer thickness estimate. *IEEE Trans Geosci Remote Sens* 7(3):435–439.
23. Wilcox BB, Robinson MS, Thomas PC, Hawke BR (2005) Constraints on the depth and variability of the lunar regolith. *Meteorit Planet Sci* 40(5):695–710.
24. Hiesinger H, Head JW, Wolf U, Jaumann R, Neukum G (2010) Ages and stratigraphy of lunar mare basalts in Mare Frigoris and other nearside maria based on crater size-frequency distribution measurements. *J Geophys Res* 115(E3):E03003.
25. Neukum G, Horn P (1976) Effects of lava flows on lunar crater populations. *Moon* 15(3-4):205–222.
26. Hiesinger H, Head JW, Wolf U, Jaumann R, Neukum G (2002) Lunar mare basalt flow units: Thicknesses determined from crater size-frequency distributions. *Geophys Res Lett* 29(8):L014847.
27. Giguere TA, Taylor GJ, Hawke BR, Lucey PG (2000) The titanium contents of lunar mare basalts. *Meteorit Planet Sci* 35(1):193–200.
28. Gillis JJ, Jolliff BL, Elphic RC (2003) A revised algorithm for calculating TiO_2 from Clementine UVVIS data: A synthesis of rock, soil, and remotely sensed TiO_2 concentrations. *J Geophys Res* 108(E2):5009–5016.
29. Ono T, et al. (2009) Lunar radar sounder observations of subsurface layers under the nearside maria of the Moon. *Science* 323(5916):909–912.
30. Oshigami S, et al. (2014) Mare volcanism: Reinterpretation based on Kaguya Lunar Radar Sounder data. *J Geophys Res Planets* 119(5):1037–1045.